Accepted Manuscript

Title: Sagging Resistance of Warm Formed Aluminum Brazing Sheet

Authors: M.J. Benoit, R. Kaur, M.A. Wells, H. Jin, B. Shalchi Amirkhiz, S. Winkler

Please cite this article as: Benoit, M.J., Kaur, R., Wells, M.A., Jin, H., Amirkhiz, B.Shalchi, Winkler, S., Sagging Resistance of Warm Formed Aluminum Brazing Sheet.Journal of Materials Processing Technology https://doi.org/10.1016/j.jmatprotec.2017.11.041

This is a PDF f le of an unedited manuscript that has been accepted for publication. As a service to our customers we are providing this early version of the manuscript. The manuscript will undergo copyediting, typesetting, and review of the resulting proof before it is published in its f nal form. Please note that during the production process errors may be discovered which could affect the content, and all legal disclaimers that apply to the journal pertain.

Sagging Resistance of Warm Formed Aluminum Brazing Sheet

M.J. Benoit[1], R. Kaur[1], M.A. Wells[1], H. Jin[2], B. Shalchi Amirkhiz[2], S. Winkler[3]

[1]*Department of Mechanical and Mechatronics Engineering, University of Waterloo, 200 University Ave. W., Waterloo, ON, Canada, N2L 3G1*
[2]*CanmetMATERIALS, 183 Longwood Rd S, Hamilton, ON, Canada, L8P 0A5*
[3]*Dana Canada Corporation, 656 Kerr St., Oakville, ON, Canada, L6K 3E4*

Abstract Interrupted tensile tests, performed between room temperature (RT) and 250°C, were used to simulate warm forming of an AA3003/AA4045 brazing sheet. Brazing performance was predicted from sagging distance measurements after a thermal cycle. The sagging distance as a function of strain for sheets strained at 150°C was similar to that of RT strained samples, while the sagging distances were large at all levels of applied strain for sheets strained at 200°C and 250°C. Large sagging distances were correlated with the occurrence of liquid film migration during simulated brazing and a recovered substructure in the core alloy, while small sagging distances were associated with a coarse, recrystallized core alloy. The poor brazing performance of sheets formed above 150°C was proposed to be due to a reduction in work hardening during forming, resulting in a recovered, rather than recrystallized, microstructure which is susceptible to liquid film migration.

Keywords: Warm Forming, Brazing, Sagging Distance, Liquid Film Migration (LFM), Recrystallization, Strain Induced Boundary Migration (SIBM)

1.0   Introduction

Since the 1970's, automotive heat exchanger production has largely been achieved by controlled atmosphere brazing of aluminum (Al) alloy sheets and tubes, as vehicle producers sought cost and weight savings (Zhao & Woods, 2013). During production, Al brazing sheets are formed to the required geometry, assembled with other components, and are passed through a brazing furnace. The Al sheets are multi-layered, consisting of at least two Al alloy layers. The core layer is often a manganese (Mn)-rich AA3xxx series alloy, which provides strength to the assembly, while the clad layer is a silicon (Si)-rich AA4xxx series alloy. The high Si content of the clad alloy sufficiently depresses the melting temperature such that, during brazing, the clad alloy is either partially or fully liquid, while the core alloy remains solid. After removal from the furnace, the assembly is fully joined, with the re-solidified clad alloy serving as the filler metal for the brazed joints.

Unfortunately, as noted by Bolt et al. (2001) cold rolled Al alloy sheets are known to have relatively poor formability compared with other conventional materials used in automotive applications, such as sheet steel. As noted by Zhao and Woods (2013), Al alloy sheet deformation continues to be a concern for heat exchanger manufacturers as they strive to use progressively thinner sheets. Warm forming, where sheets are heated to below their

recrystallization temperature during forming, has shown to be an effective method to improve Al alloy formability. The majority of previous warm forming studies have focussed on AA5xxx and AA6xxx series alloys used in structural automotive applications. As outlined in a review by Tebbe and Kridli (2004), a number of past studies have demonstrated the potential to form components with complex geometries from AA5xxx and AA6xxx alloys through the use of warm forming. Toros et al. (2008) also noted the improvements in formability of AA5xxx alloys shown in past studies by forming between 200°C and 300°C. Recently however, it has been shown that warm forming also improves the formability of multi-layered Al brazing sheets. Bagheriasl et al. (2014) demonstrated that a plate component with a drawn cup feature, which required multiple forming steps at room temperature, was able to be formed in a single step using warm forming with a die temperature between 250°C and 300°C. It was further shown by Bagheriasl and Worswick (2015) that the limiting strain before failure of an Al brazing sheet could be increased by over 200% when the forming temperature was increased to 200°C.

While warm forming appears to be a promising technique to improve formability of Al brazing sheet, the implications of the process on subsequent brazing are, as of yet, unexplored. The co-existence of liquid clad and solid core alloys during brazing leads to interactions between the two alloys, such as penetration of liquid clad into the core, which depletes the amount of filler metal available for brazing and impairs the properties of the core alloy. One interaction of particular interest for strained Al brazing sheets is the phenomenon of liquid film migration (LFM), where liquid clad penetrates the core and progresses as a film, leaving a solid solution consistent with the equilibrium solidus composition at the brazing temperature in the area behind the film (Yoon & Huppmann, 1979). LFM in strained Al brazing sheet was first characterized by Woods (1997), where it was shown that the braze filler metal flow, a measure of brazeability, was drastically reduced in a 5% cold worked sample compared to a fully annealed specimen. Yang and Woods (1997) then demonstrated that the measured depth of LFM attack into the core layer had a non-linear dependence on the level of applied strain; the depth of LFM attack increased with applied strain up to 7.5%, but then decreased with the further application of strain. A number of LFM driving forces were proposed, but the dominant one was not conclusively determined. Recently, Wittebrood (2009) re-evaluated the proposed driving forces for LFM, and concluded that the reduction of stored deformation energy in the core alloy, through the elimination of dislocation sub-structures by the migrating liquid film, was the most viable explanation, despite a lack of direct evidence. Given the dependence of LFM on applied strain, it is critical to understand how the occurrence of LFM changes with changes in forming conditions, such as a shift to warm forming. The objective of the current study was to determine if warm

forming would negatively impact the brazing performance of multi-layered Al brazing sheet, compared to room temperature strained sheets, which was assessed by the commonly used sagging test.

2.0 Experimental

2.1 Materials and Sample Preparation

Industrially produced Al brazing sheet comprised of a modified AA3003 core alloy and a single AA4045 clad alloy layer was used in the current study. The alloy compositions are given in Table 1. The core alloy composition was measured using inductively coupled plasma optical emission spectrometry (ICP-OES) after removing the clad alloy by chemical etching with sodium hydroxide solution. The core alloy surface was masked prior to etching, and the sheet was left in solution until at least 30µm of sheet thickness was dissolved. The clad layer composition was then calculated by performing ICP-OES on the full brazing sheet and subtracting the weighted core alloy composition. The sheets were supplied in the fully annealed condition (i.e. O temper), with a measured overall sheet thickness of 202.7±1.5µm and clad layer thickness of 25.8±1.2µm. The sheet cross section in the as-received condition is shown in Fig. 1; the core alloy is characterized by a mixture of elongated grains remaining from rolling during processing and smaller, rounded grains from the annealing heat treatment.

Table 1 Composition in wt% of Al alloys used in the brazing sheet (bal. Al).

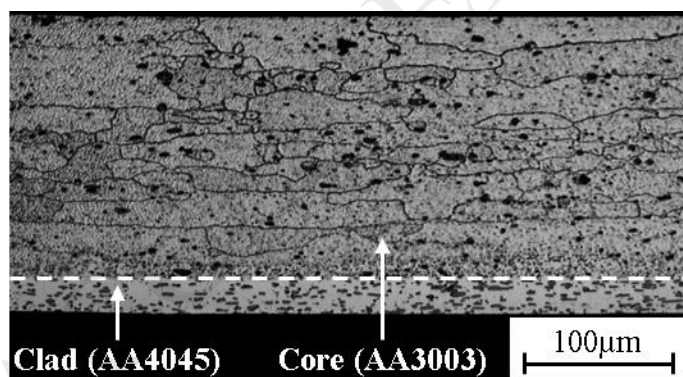| Sheet Alloy	Si	Mn	Cu	Fe	Others
Clad (AA4045)	9.19	-	0.11	0.10	≤0.08
Core (AA3003)	0.18	0.86	0.64	0.33	≤0.08

Fig. 1 Cross section of as-received brazing sheet.

Tensile specimens with a gauge length and width of 19.1 mm (3/4in) and 12.7mm (1/2in), respectively, were strained along the sheet rolling direction. To simulate warm forming, a tensile tester (Instron model 5697) equipped with a furnace (Instron model 3119-606) was used to strain the tensile specimens at room temperature (RT), 150°C,

200°C, and 250°C. Prior to beginning the test, the sample temperature was allowed to equilibrate in the furnace. Samples were strained to pre-determined levels of engineering strain between 2-12%, at an average strain rate of $6.6 \times 10^{-4} s^{-1}$, before the test was terminated. Strain was measured using an MTS video extensometer and two points along the gauge length.

2.2 Sagging Test

The sagging test is a common technique used to predict the brazing performance of Al brazing sheets. After clamping one end of a sample in a fixture and exposing the fixture to a simulated brazing cycle, the deflection of the sample's free end is measured. As noted by Zhao and Woods (2013), a strong resistance of the brazing sheet to sagging is desirable, as a large sagging distance indicates that the sheet will lose its rigidity during brazing and the assembly may collapse under its own weight. In the current study, sagging test samples were prepared by shearing one grip end off of the strained tensile specimens. The opposite end of the specimen was clamped in the sagging test fixture such that 23mm of the strained specimen was cantilevered over the test fixture. A schematic diagram of the test set-up can be seen in Fig. 2.
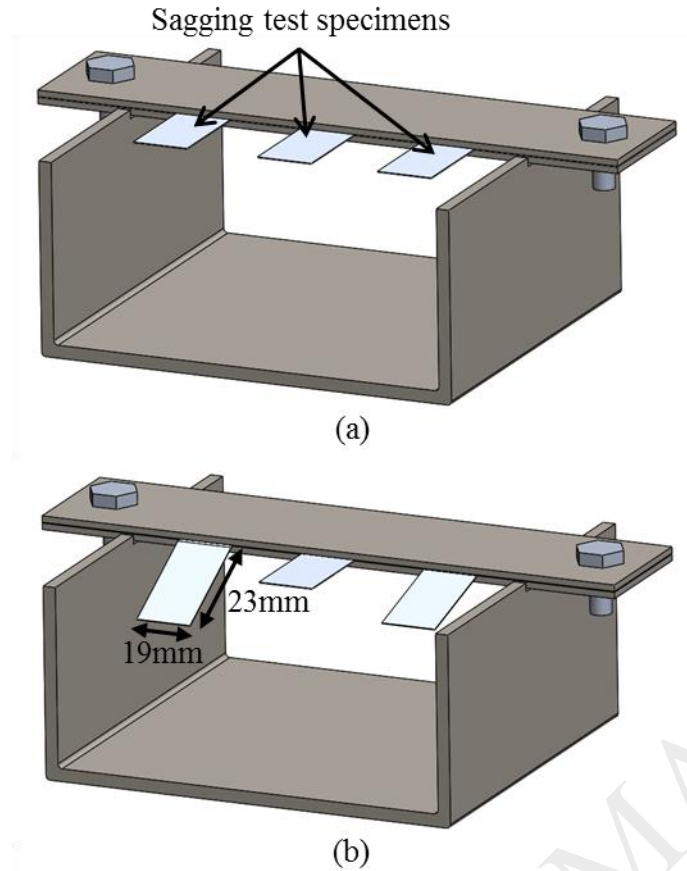
Fig. 2 Schematic representation of the sagging test fixture and samples (a) before and (b) after a simulated brazing cycle.

A Thermo Scientific Lindberg/Blue M Moldatherm box furnace was used to simulate an industrial brazing cycle for the sagging test. Prior to heating, the furnace was backfilled with high purity (99.999%) nitrogen gas, which continued to be flowed through the furnace throughout the test. Prior to performing the sagging tests, the furnace temperature profile was calibrated using as-received brazing sheet samples instrumented with thermocouples at both the free and clamped ends of the sample, attached to the core side of the sheet using thermal paste. The furnace controller was set to 598°C for the simulated brazing heat treatment; from the calibration data, the average maximum temperature at the free end of the samples was 601°C, while the average temperature at the clamped end was slightly higher (605°C) due to the thermal mass of the test fixture. After complete solidification of the clad alloy during cooling (550°C), the nitrogen gas flow was stopped, and the furnace door was opened when the sample temperature reached 525°C to rapidly cool the samples. The average heating rate from RT to the peak temperature was approximately 15°C/min, while the cooling rate up to the point where the furnace door was opened was approximately 10°C/min.

The measured sample temperature profile over the entire test is given in Fig. 3a, and a magnified view of the sample temperature over the range where clad alloy is liquid is given in Fig. 3b.
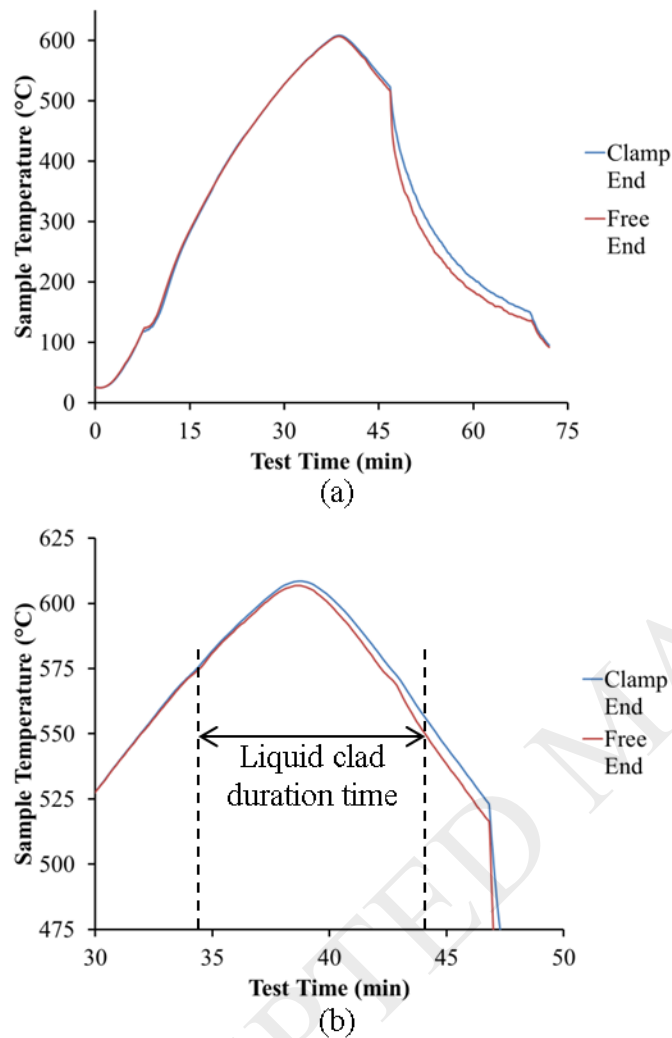

Fig. 3 Measured temperature profile at both ends of the brazing sheet sample over (a) the entire test duration and (b) the segment of the heating profile when liquid clad is present. The liquid duration time for the free end of the sample is indicated.

As previously noted, it is important to understand how a change in forming conditions affects metallurgical interactions between the liquid clad and solid core during brazing, such as LFM. Thus, it was important to have an estimate of the time over which LFM could occur, which is the time between the onset of clad melting to the end of clad solidification (Fig. 3b). The clad liquid duration time (LDT) at the clamped and free ends of the samples at each of the three specimen locations on the sagging test fixture was estimated using the calibration data (Fig. 4). The LDT

was longer at the clamped end of the sample due to the proximity to the test fixture. The average LDT was similar across the three fixture locations (within 1 standard deviation), for both the clamped and free ends of the samples.
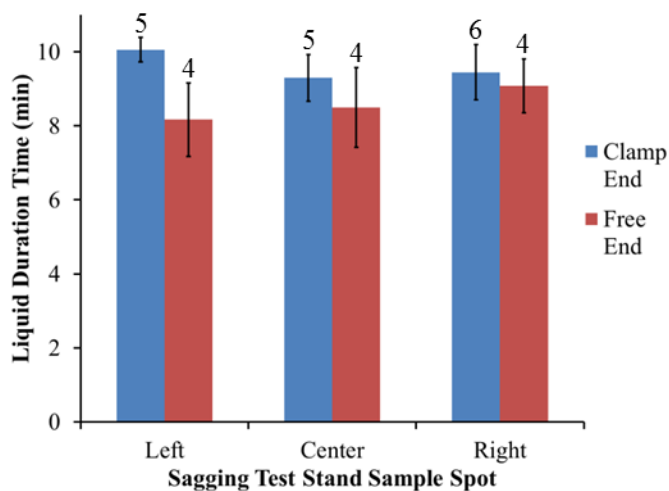

Fig. 4 LDT estimated from thermocouple data at the clamped and free ends of the sample at each fixture location. The number of measurements used to determine the LDT are indicated above each estimate.

After removing the test fixture from the furnace, the deflection of the free end of the samples was measured. Two replicates were performed for each forming temperature-strain combination, where the second replicates were tested in a different clamp location than the first replicates, and the test order was completely randomized to reduce the effect of lurking variables.

2.3 Microstructure and Composition Analysis

After the sagging test, samples were mounted and prepared for microscopy by standard metallographic grinding and polishing. The sheet microstructure was revealed by etching the cross sections with Keller's reagent. A Philips XL30 scanning electron microscope (SEM) equipped with energy dispersive x-ray spectroscopy (EDS) was used to estimate the local chemical composition across the clad-core interface after the sagging test, using an accelerating voltage of 15kV.

To investigate the driving force for LFM, transmission electron microscopy (TEM) analysis was conducted across the clad-core interface before and after simulated brazing for a number of forming conditions. The brazing cycle was simulated by punching 4.8mm (3/16in) discs from the gauge length of newly prepared strained samples, placing the discs within a controlled atmosphere furnace, and holding at 600°C for 10min. All heating and cooling was performed at 20°C/min below 500°C and 10°C/min above 500°C. The samples were then mounted along the

direction of applied strain, ground, and polished. An FEI Helios NanoLab 650 focussed ion beam (FIB) microscope was used to prepare lift out samples across the clad-core interface. TEM analysis was performed using an FEI Tecnai Osiris microscope, using an accelerating voltage of 200kV. Imaging was performed using bright field scanning TEM (BF-STEM) mode, where the electron beams were focussed to a probe and scanned in a raster pattern across the imaging area.

3.0   Results

The brazing sheet true stress-strain curves are given in Fig. 5 for all forming temperatures investigated, up to the maximum strain studied. The material flow stress and level of work hardening both decreased with increasing forming temperature.
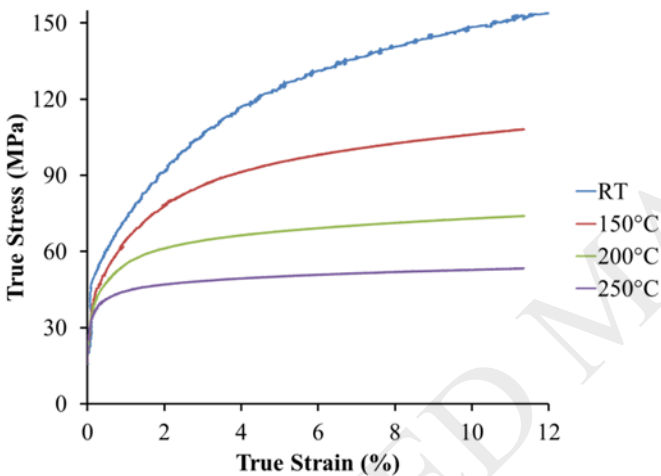

Fig. 5 Brazing sheet true stress-strain curves for a number of forming temperatures.

The measured sagging distances after exposure to the simulated brazing treatment as a function of strain are given in Fig. 6. For all forming temperatures, the sagging distance initially increased with applied strain, but then decreased with the further application of strain once a threshold level of strain was reached. The decrease in sagging distance as a function of strain was most rapid for RT strained samples, followed by samples strained at 150°C; at the highest levels of strain studied, the sagging distance of samples formed at RT and 150°C were similar. The sagging distance for samples strained at 200°C and 250°C remained large compared to those of samples formed at RT and 150°C, even at the highest levels of strain. The data in Fig. 6 are the average of two measurements for each forming condition, plotted with error bars representing the standard deviation of the measurements. Overall, the experimental repeatability was excellent, where differences between sagging distance measurements for a given forming condition

were at maximum 2mm. The only exceptions were the RT-4% and 150°C-4% forming conditions, where the differences in sagging distance measurements were 5mm and 7.5mm, respectively. The discrepancy in these measurements was suspected to be due to the fact that these forming conditions correspond to the peak sagging distance for their respective forming temperatures, separating regions where the sagging distance increased with applied strain from where sagging distance decreased with applied strain, and will be discussed further in the subsequent section.
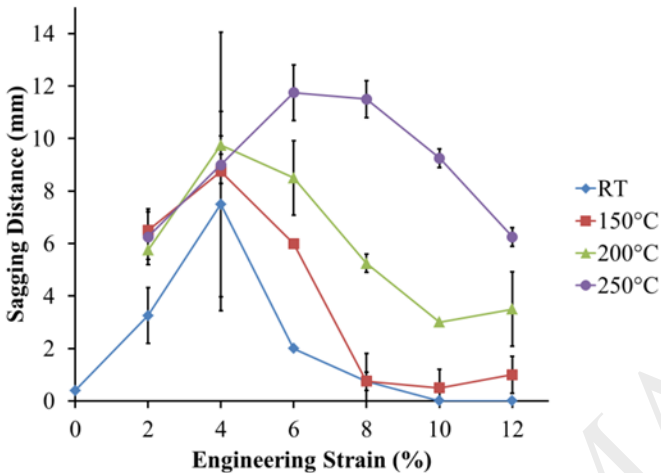

Fig. 6 Brazing sheet sagging distance as a function of strain for a number of forming temperatures.

Sheet microstructures after exposure to the sagging test (i.e. simulated brazing treatment) are shown in Fig. 7 to Fig. 9. It can be seen from the micrographs that for forming conditions where the sagging distance was large, liquid clad alloy attack on the core occurred during the sagging test, leaving large precipitate free grains at the sheet surface. Furthermore, the corresponding core alloy microstructures were characterized by small grains aligned along the direction of applied strain. Conversely, the microstructures of forming conditions corresponding to low sagging distances (i.e. >4% at RT and >6% at 150°C) were characterized by coarse recrystallized core grains, with grain sizes approaching the sheet thickness, and minimal, if any, instances of clad alloy attack on the core alloy.
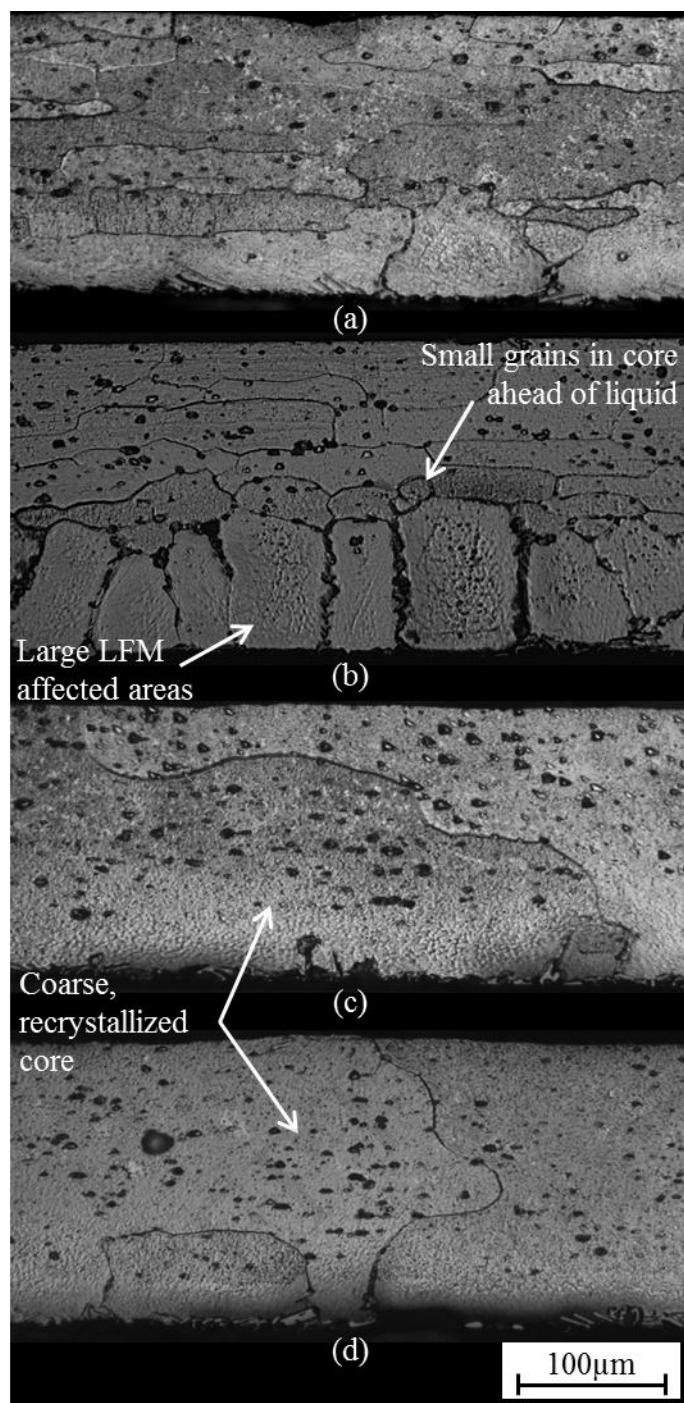
Fig. 7 Post-sagging test microstructures for sheets strained at RT to (a) 2%, (b) 4%, (c) 6%, and (d) 10% engineering strain.
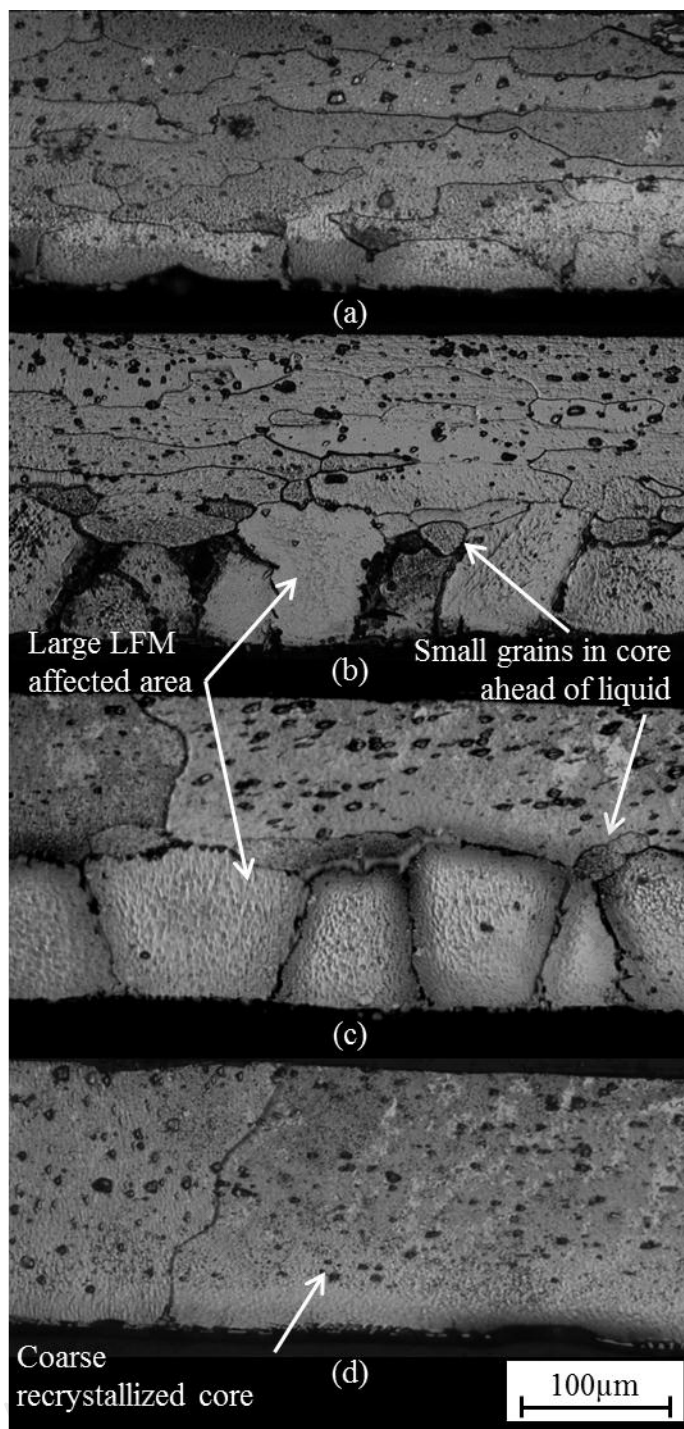
Fig. 8 Post-sagging test microstructures for sheets strained at 150°C to (a) 2%, (b) 4%, (c) 6%, and (d) 10% engineering strain.
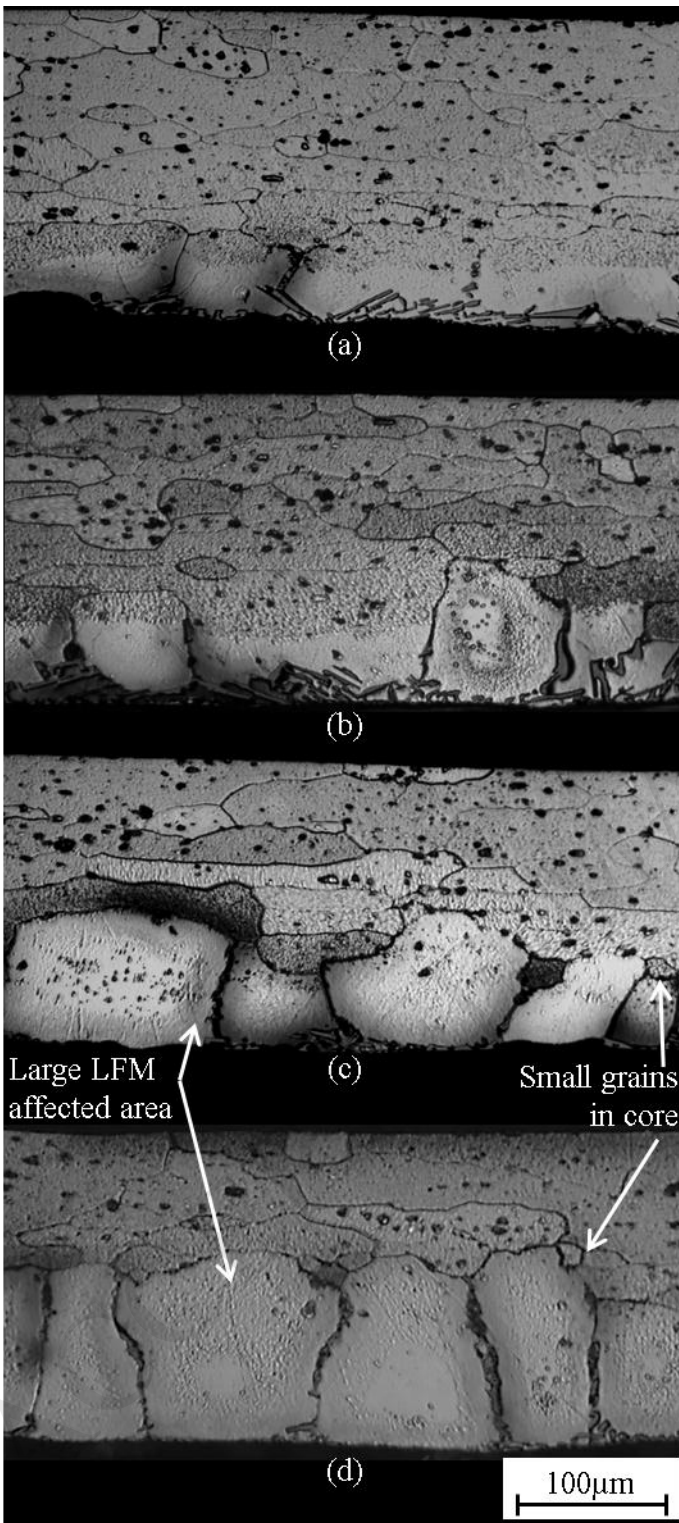
11

Fig. 9 Post-sagging test microstructures for sheets strained at 250°C to (a) 2%, (b) 4%, (c) 6%, and (d) 10% engineering strain.

EDS composition measurements through the sheet thickness after the sagging test for two forming conditions where severe liquid clad attack was observed are given in Fig. 10. The data have been overlaid on SEM images of the microstructure from which they were obtained, and all measurements were taken along a line corresponding with the abscissa in each plot. It was found that the large surface grains which were correlated with large sagging distances had a Si content around the maximum solubility in Al, consistent with LFM, and a diffusion profile ahead of these grains into the remaining core.
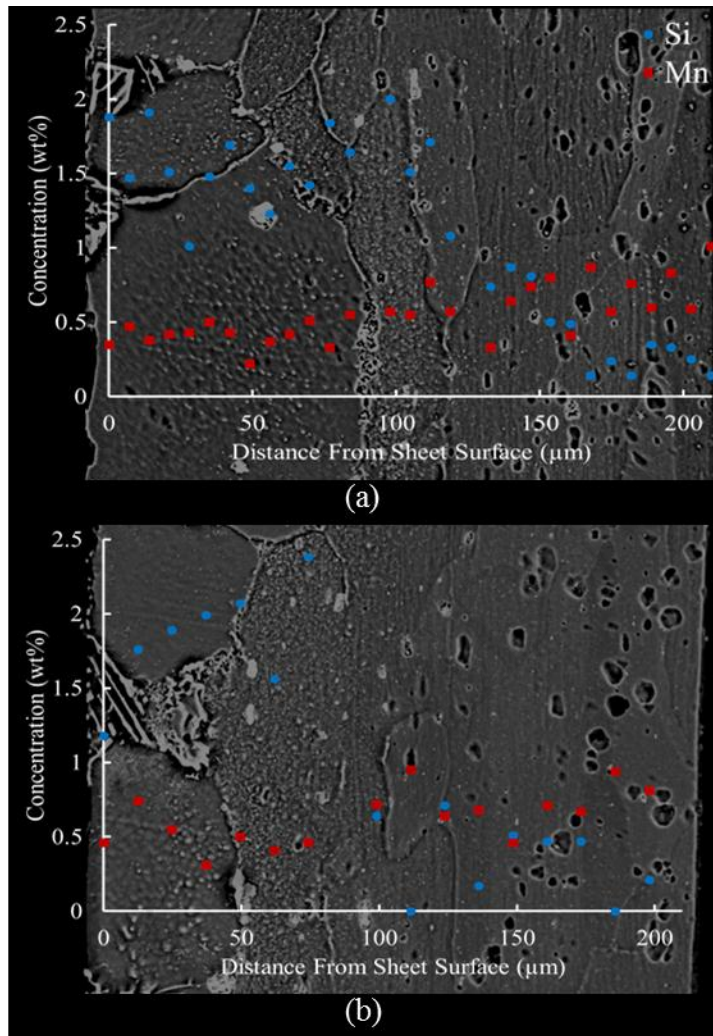

Fig. 10 Through-thickness measurements after the sagging test for (a) RT-4% and (b) 250°C-10% forming conditions. Measurements were taken along a line coinciding with the abscissa in both plots.

The BF-STEM images from the clad-core interface are given in Fig. 11 for a number of forming conditions before and after a simulated brazing heat treatment. In all images, the core alloy is toward the top of the image. Dislocations cells were observed in all forming conditions prior to the brazing heat treatment, due to the applied strain

(Fig. 11a-c). After the brazing heat treatment, the dislocation density in the RT-10% forming condition was significantly reduced (Fig. 11e), indicating that the coarse core grain structure observed in Fig. 7d was in fact a recrystallized microstructure. The presence of sub-grains in the core for the RT-4% and 250°C-10% forming conditions (Fig. 11d and f) indicate that for conditions where LFM occurred during brazing, the core alloys did not recrystallize.
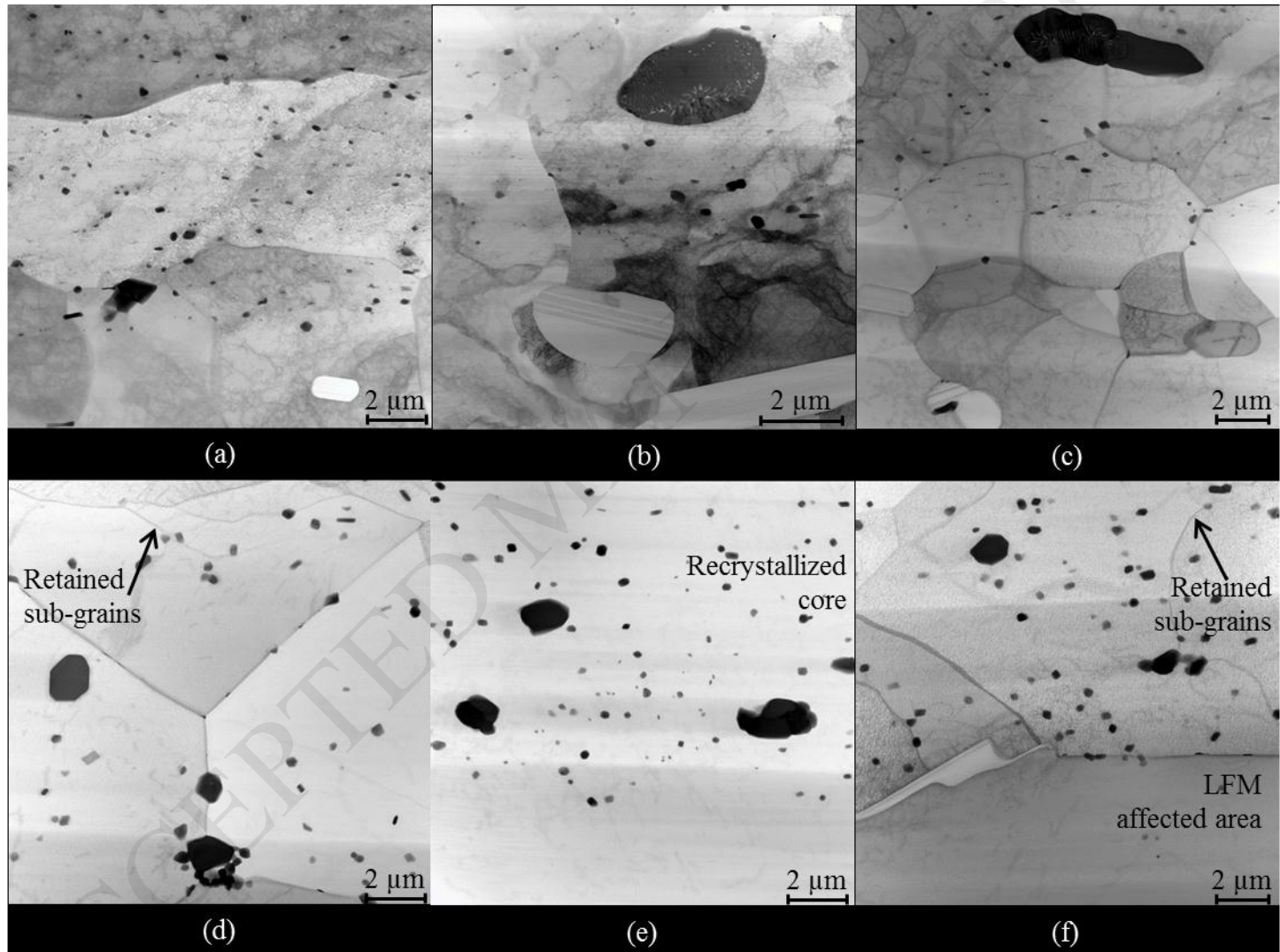

Fig. 11 BF-STEM images at the clad-core interface (a-c) before and (d-f) after a simulated brazing cycle for (a, d) RT-4%, (b, e) RT-10%, and (c, f) 250°C-10% forming conditions.

4.0 Discussion

The trend in the sagging distance as a function of RT applied strain in the current investigation was in excellent agreement with past studies investigating the effect of deformation on clad-core interactions during brazing.

A non-linear relationship between various parameters used to quantify LFM and applied strain have been documented in a number of past studies. Yang and Woods (1997) reported an increase in the depth of LFM attack with increasing strain, up to 7.5% strain, but a subsequent decrease in LFM depth with further increased in strain. Similarly, Wittebrood et al. (1998) showed the same trend in LFM depth as a function of strain, where the maximum depth of attack occurred at 3% strain, and the inverse relationship for braze joint fillet area (i.e. the smallest fillet area occurred at 3% strain). Wittebrood et al. (2000) found that the ratio of clad alloy solidification energy after a simulated brazing cycle to the clad alloy melting energy, which indicates the amount of liquid clad alloy not consumed by LFM during brazing, had a non-linear relationship with applied strain, where the ratio was minimized in sheets strained to between 2%-4%, depending on the initial grain size. Finally, Yoon et al. (2001) showed a non-linear relationship between sheet sagging distance and the rolling reduction of the brazing sheet thickness during production, where the sagging distance was high at low reductions, small at intermediate reductions, and then increased again at the high levels of sheet thickness reduction. Yoon et al. further showed that the sagging distance was strongly correlated with the average depth of erosion of the core by the liquid clad during brazing. Thus, the sagging distance is a suitable parameter to predict the brazing performance of warm formed brazing sheets. The past studies noted above have demonstrated that a coarse, recrystallized core microstructure is ideal to prevent liquid clad attack during brazing. First, recrystallization reduces stored deformation energy in the core alloy, thus reducing the driving force for liquid clad penetration, as originally proposed by Woods (1997) and later re-visited by Wittebrood (2009). Second, a coarsened recrystallized grain size is preferred, as larger grains reduce the number of grain boundaries intersecting the liquid clad, which provide high diffusivity paths for clad penetration. Tu et al. (2011) demonstrated the benefits of a coarse recrystallized microstructure by showing a drastic reduction in sagging distance when sheet processing parameters were adjusted to result in a recrystallized post-braze core alloy, but a subsequent rise in sagging distance when the processing parameters were further adjusted to result in a recrystallized post-braze microstructure with a finer grain size. Bellier and Doherty (1977) showed that recrystallization in moderately strained Al alloys, such as those in the current investigation, occurs through the process of strain induced boundary migration (SIBM), as opposed to nucleation and growth of new grains. The driving pressure for SIBM is a difference in dislocation densities across grain boundaries, such that above a critical difference, a boundary will bulge into the grain with higher dislocation density, reducing the dislocation density behind the migrating boundary. Thus, during SIBM certain grains preferentially grow at the expense of others, leading to a coarsened grain structure. The benefit of such a core alloy microstructure for brazing

performance was observed in Fig. 7c and d and Fig. 8d, where negligible, if any, liquid clad attack was observed, and the corresponding sagging distance was low.

Forming conditions in the current investigation with large sagging distances were correlated with liquid clad attack on the core during brazing, where the current results revealed that the attack was due to the phenomenon of LFM. According to Yoon and Huppmann (1979), dissolution of the base metal occurs directly ahead of the liquid film, and is re-precipitated as a solid solution behind the film as the film migrates. As noted by Barker and Purdy (1998), the re-precipitated region should be in equilibrium with the solidus composition at the brazing temperature. The composition data in Fig. 10 indicated that the LFM grains had a Si concentration close to the maximum solubility in Al, and a Si diffusion profile ahead of the advancing film was observed, as was also noted by Wittebrood (2009).

As the sagging distance had a non-linear relationship with applied strain, and large sagging distances were correlated with the occurrence of LFM, the occurrence of LFM also has a non-linear relationship with applied strain. Recently, Wittebrood (2009) suggested that LFM in strained Al brazing sheet is a special case of the more general phenomenon, which he denoted strain induced LFM (SILFM), where the liquid clad film progresses into the core to reduce stored deformation energy. As the film progresses through the core, the dislocation density (i.e. stored deformation energy) is reduced, since the liquid film cannot support the dislocations. The driving pressure (P) for SILFM was proposed to be:

$$P = \alpha \rho_f G b^2 / 2 \ + 2\gamma_b / R \text{ (eq 1)}$$

where ρ_f is the dislocation density in the core ahead of the liquid film, G is the shear modulus, b is the Burgers vector, γ_b is the grain boundary energy, R is the radius of the bulging grain, and α is a constant. The driving pressure for SILFM is directly proportional to the dislocation density ahead of the liquid film; thus, both SIBM and SILFM are driven by the reduction of stored deformation energy. When SIBM occurs before the onset of clad alloy melting during the brazing cycle, the driving pressure for SILFM is reduced and liquid clad attack is minimized (Wittebrood A. , 2009). The BF-STEM images in Fig. 11 provided compelling evidence for the strain induced driving force for LFM and the competition between SIBM and SILFM during brazing. When the dislocation density in the core is sufficiently high prior to brazing, the core recrystallizes early in the brazing cycle, eliminating core dislocations and preventing SILFM (Fig. 11e). On the other hand, when the dislocation density is not sufficiently high to initiate SIBM, the retained dislocations provide the driving pressure for SILFM, as suggested by the sub-grains observed directly ahead of the liquid clad front in Fig. 11d and f.

16

The interplay between SIBM and SILFM, and the consequent effect on sagging distance, was demonstrated by further investigation of the RT-4% and 150°C-4% forming conditions. As noted previously, these were the only forming conditions with a large discrepancy in sagging distance measurements and were the turning point in their respective sagging distance curves. The sagging distances corresponding to the microstructures in Fig. 7b and Fig. 8b were 10mm and 12.5mm, respectively. In both cases, a non-recrystallized core and SILFM were observed. The sagging distance for the second replicate for both of these forming conditions was 5mm, and the corresponding microstructures are given in Fig. 12. In both cases, SILFM occurred during the sagging test, with some small non-recrystallized grains ahead of the affected area, which lead to the relatively high sagging distance (5mm). Beyond the SILFM affected area however, the core alloy consisted of coarse recrystallized grains, which prevented further progression of SILFM. As the sheets are polycrystalline, some grains would be favourably oriented with the direction of applied strain. Near the critical level of applied strain, these grains would have sufficient stored energy to initiate SIBM, but SILFM could still occur locally in other regions of the sheet where the stored energy is below the critical level. Such localized SILFM was also noted by Wittebrood (2009). It is believed that the balance between SIBM and SILFM for the same forming condition lead to the variability in sagging distance observed at the critical level of applied strain.
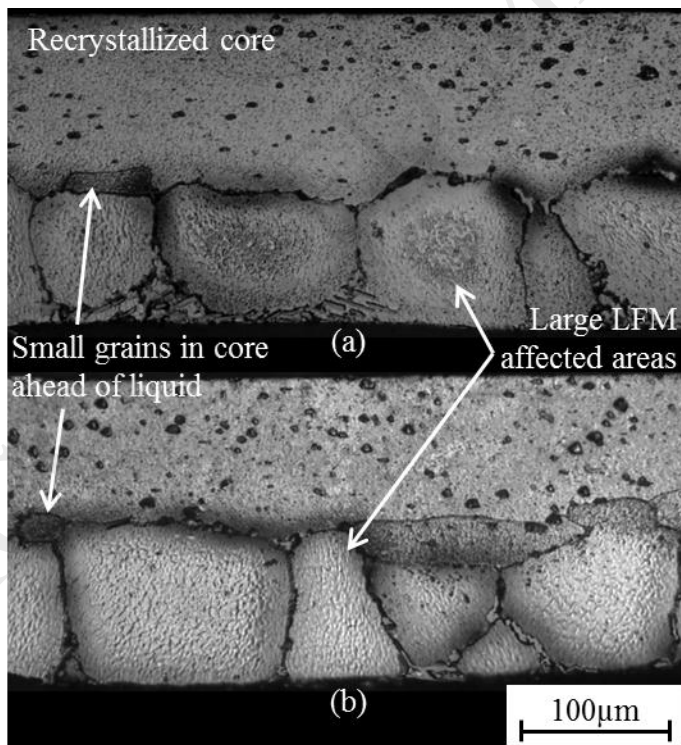

Fig. 12 Post-sagging test microstructures for the second replicate corresponding to (a) RT-4% and (b) 150°C-4% forming conditions.

To relate the sagging distance and microstructure results to warm forming, the dislocation density in the sheet prior to brazing is approximated by (Humphreys & Hatherly, 2004):

$$\rho = (\sigma/cGb)^2 \quad \text{(eq 2)}$$

where σ is the brazing sheet flow stress, and c is a constant. By combining eq 1 and eq 2, the driving pressure for SILFM is proportional to the square of the material flow stress; thus, from Fig. 5, the driving pressure for SILFM should change with changes in forming temperature. In theory then, above a critical flow stress (e.g. the flow stress corresponding to RT-6%) SIBM occurs within the sheet, but up to this critical value, the driving pressure for SILFM would rise with the square of the flow stress. During warm forming, the material flow stress and work hardening were reduced from their RT levels (Fig. 5). Thus, the driving force for SILFM increases more gradually during warm forming, but it becomes increasingly difficult to reach the critical flow stress to cause SIBM, and the regime of strains over which SILFM can occur is extended. Coupling the SILFM driving pressure to the material flow stress is however, only a convenient approximation to relate the metallurgical phenomenon to warm forming, and is not without some discrepancy. For example, the RT-4% microstructure (Fig. 7b) was non-recrystallized, while a coarsened grain structure was observed for 150°C-6% (Fig. 8c), despite a lower flow stress in the latter case. One explanation for the discrepancy is that eq 1 and eq 2 relate the SILFM driving pressure to the dislocation density, even though it would be more accurately related to the energy associated with a sub-grain structure (Fig. 11d and f). The sub-grains may nucleate and grow as a result of dynamic recovery during warm forming or during the brazing cycle, however a complete discussion of recovery kinetics is beyond the scope of the current work. Another possible explanation for the discrepancy is that the driving pressure in eq. 1 is related to the dislocation density ahead of the film (i.e. in the core), while the flow stress curves in Fig. 5 were for the multi-layered brazing sheet. However, bare core alloy with the same processing history as the multi-layered brazing sheet was not available for study.

5.0 Conclusions

The brazing performance of warm formed Al brazing sheet was assessed using the sheet sagging distance. Sagging distance measurements were corroborated with microstructural changes during simulated brazing. The experimental results have shown:

1. The sagging distance of sheets formed at room temperature and 150°C were similar, suggesting similar brazing performance, and displayed a non-linear dependence on applied strain. Conversely, the sagging

18

distance of sheets formed at 200°C and 250°C remained elevated even at high levels of applied strain, indicating poor brazing performance.

2. Large sagging distances were strongly correlated with a non-recrystallized core alloy and the occurrence of liquid film migration during brazing. On the other hand, forming conditions with small sagging distances coincided with coarse, recrystallized core grains.

3. TEM imaging revealed a recovered sub-grain structure ahead of the liquid front in forming conditions where liquid film migration occurred; this finding provided strong evidence for the recently proposed strain induced driving force for the liquid film migration phenomenon.

Acknowledgements

References

Bagheriasl, R., & Worswick, M., 2015. Formability of AA3003 brazing sheet at elevated temperatures: limiting dome height experiments and determination of forming limit diagrams. Int. J. Mater. Form. 8, 229-244.

Bagheriasl, R., Ghavam, K., & Worswick, M., 2014. Formability improvement with independent die and punch temperature control. Int. J. Mater. Form. 7, 139-154.

Barker, S. W., & Purdy, G. R., 1998. On liquid film migration in aluminum-copper alloys. Acta Mater. 46, 511-524.

Bellier, S. P., & Doherty, R. D., 1977. The structure of deformed aluminium and its recrystallization-investigations with transmission Kossel diffraction. Acta Metall. 25, 521-538.

Bolt, P. J., Lamboo, N. A., & Rozier, P. J., 2001. Feasibility of wam drawing of aluminium products. J. Mater. Process. Technol. 115, 118-121.

Humphreys, F. J., & Hatherly, M., 2004. Recrystallization and related annealing phenomena, second ed. Elsevier, Oxford, pp 17.

Tebbe, P. A., & Kridli, G. T., 2004. Warm forming of aluminium alloys: an overview and future directions. Int. J. Mater. Prod. Technol., 21, 24-40.

Toros, S., Ozturk, F., & Kacar, I., 2008. Review of warm forming of aluminum-magnesium alloys. J. Mater. Process. Technol. 207, 1-12.

Tu, Y., Liu, X., Zhang, M., & Zhang, J., 2011. Improving brazeability of AA3003+Zn brazing aluminum sheets by final annealing. Adv. Mater. Res. 197-198, 1555-1560.

Wittebrood, A., 2009. Microstructural Changes in Brazing Sheet due to Solid-Liquid Interaction. PhD Thesis, Delft University of Technology, Delft, Netherlands.

Wittebrood, A. J., Benedictus, R., & Vieregge, K., 1998. Study of liquid film migration in o-temper aa3005 brazing sheet. In Proceedings of the 6th International Conference on Aluminum Alloys, The Japan Institute of Light Metals,Toyohashi, Japan, pp. 1459-1464.

Wittebrood, A., Kooij, C. J., & Vieregge, K., 2000. Grain Boundary Melting or Liquid Film Migration in Brazing Sheet. Mater. Sci. Forum. 331-337, 1743-1750.

Woods, R., 1997. Liquid Film Migration During Aluminum Brazing. SAE Technical Paper 971848. DOI:10.4271/971848

Yang, H. S., & Woods, R. A., 1997. Mechanisms of Liquid Film Migration (LFM) in Aluminum Brazing Sheet. SAE Technical Paper 971849. DOI:10.4271/971849

Yoon, D. N., & Huppmann, W. J., 1979. Chemically driven growth of tungsten grains during sintering in liquid nickel. Acta Metall. 27, 973-977.

Yoon, J. S., Lee, S. H., & Kim, M. S., 2001. Fabrication and brazeability of a three-layer 4343/3003/4343 aluminum clad sheet by rolling. J. Mater. Process. Technol., 111, 85-89.

Zhao, H., & Woods, R., 2013. Controlled atmosphere brazing of aluminum. In D. Sekulic (Ed.), Advances in brazing - science, technology and applications. Woodhead Publishing, Cambridge, pp. 280-292.

List of Figure Captions

Fig. 1 Cross section of as-received brazing sheet.

Fig. 2 Schematic representation of the sagging test fixture and samples (a) before and (b) after a simulated brazing cycle.

Fig. 3 Measured temperature profile at both ends of the brazing sheet sample over (a) the entire test duration and (b) the segment of the heating profile when liquid clad is present. The liquid duration time for the free end of the sample is indicated.

Fig. 4 LDT estimated from thermocouple data at the clamped and free ends of the sample at each fixture location. The number of measurements used to determine the LDT are indicated above each estimate.

Fig. 5 Brazing sheet true stress-strain curves for a number of forming temperatures.

Fig. 6 Brazing sheet sagging distance as a function of strain for a number of forming temperatures.

Fig. 7 Post-sagging test microstructures for sheets strained at RT to (a) 2%, (b) 4%, (c) 6%, and (d) 10% engineering strain.

Fig. 8 Post-sagging test microstructures for sheets strained at 150°C to (a) 2%, (b) 4%, (c) 6%, and (d) 10% engineering strain.

Fig. 9 Post-sagging test microstructures for sheets strained at 250°C to (a) 2%, (b) 4%, (c) 6%, and (d) 10% engineering strain.

Fig. 10 Through-thickness EDS measurements after the sagging test for (a) RT-4% and (b) 250°C-10% forming conditions. Measurements were taken along a line coinciding with the abscissa in both plots.

Fig. 11 BF-STEM images at the clad-core interface (a-c) before and (d-f) after a simulated brazing cycle for (a, d) RT-4%, (b, e) RT-10%, and (c, f) 250°C-10% forming conditions.

Fig. 12 Post-sagging test microstructures for the second replicate corresponding to (a) RT-4% and (b) 150°C-4% forming conditions.